Biosensors and Bioelectronics 61 (2014) 639–647

Contents lists available at ScienceDirect

Biosensors and Bioelectronics

journal homepage: www.elsevier.com/locate/bios

A simple strategy for the immobilization of catalase on multi-walled carbon nanotube/poly (L-lysine) biocomposite for the detection of H_2O_2 and iodate

A.T. Ezhil Vilian [a], Shen-Ming Chen [a,*], Bih-Show Lou [b,**]

[a] Electroanalysis and Bioelectrochemistry Lab, Department of Chemical Engineering and Biotechnology, National Taipei University of Technology, No. 1, Section 3, Chung-Hsiao East Road, Taipei 106, Taiwan, ROC
[b] Chemistry Division, Center for Education, Chang Gung University, 259, Wen-Hwa 1st Road, Kwei-Shan, Tao-Yuan 333, Taiwan, ROC

ARTICLE INFO

Article history:
Received 27 February 2014
Received in revised form
8 May 2014
Accepted 10 May 2014
Available online 2 June 2014

Keywords:
Multiwall carbon nanotubes
Catalase
Direct electrochemistry
Biosensor

ABSTRACT

Herein, we report a novel third-generation H_2O_2 and IO_3^- biosensor, which was fabricated by loading catalase (CAT) onto L-lysine/multiwalled carbon nanotube (PLL/*f*-MWCNT) film modified glassy carbon electrode (GCE). The UV–visible (UV–vis) and Fourier-transform infrared (FTIR) spectra show that the catalase encapsulated in the PLL/*f*-MWCNT film can effectively retain its bioactivity. The immobilized CAT retained its bioactivity with a high protein loading of 4.072×10^{-10} mol cm^{-2}, thus exhibiting a surface-controlled reversible redox reaction, with a fast heterogeneous electron transfer rate of 5.48 s^{-1}. The immobilized CAT shows a couple of reversible and well-defined cyclic voltammetry peaks with a formal potential (E^0) of −0.471 V (vs. Ag/AgCl) in a pH 6.5 phosphate buffer solution (PBS). Moreover, the modified film exhibited high electrocatalytic activity for the reduction of hydrogen peroxide (H_2O_2). It exhibited a wide linear response to H_2O_2 in the concentration range of 1×10^{-6}–3.6×10^{-3}, with higher sensitivity (392 mA cm^{-2} M^{-1}) and a lower Michaelis–Menten constant (0.224 mM). It provided high-catalytic activity towards H_2O_2 in a shorter time (5 s), with a detection limit of 8 nM. These results indicate great improvement in the electrochemical and electrocatalytic properties of the CAT/PLL/*f*-MWCNT biosensor, offering a new idea for the design of third-generation electrochemical biosensors.

1. Introduction

In recent years, hydrogen peroxide (H_2O_2) has been widely used in various fields, including food production, textile industry, pulp and paper bleaching, manufacturing of antiseptic and disinfecting agents, pharmaceutical research, clinical, biological and environmental analysis (Wagenaar and Snijders, 2004; Mistik and Yukseloglu, 2005; Tsiafoulis et al., 2005; Prakash et al., 2009a, 2009b). H_2O_2 is generated as a by-product in the classic biochemical reactions using enzymes such as glucose oxidase, cholesterol oxidase, glutamate oxidase, urate oxidase, lactate oxidase, alcohol oxidase, lysine oxidase, oxalate oxidase, and horseradish peroxidase (Chen et al., 2013). H_2O_2 did play significant roles in regulating diverse biological processes such as immune cell activation, vascular remodeling, apoptosis, stomatal closure and root growth (Wael et al., 2012). However, high concentrations of H_2O_2 affect the human health by causing irritation to the eyes and the skin. Hence, determination of H_2O_2 in trace levels in biological and various water samples are of great importance. Various techniques, including chromatography, photometry, fluorescence and electrochemical methods have been employed for the detection of H_2O_2 (Huang et al., 2011). Among these, electrochemical techniques have the advantages of good selectivity and sensitivity, short assay times, and low cost of analysis (Chen et al., 2012).

Iodine, a micronutrient present in the thyroid gland, is considered to be a significant biomolecule for physiological processes in human metabolism (Yang et al., 1991), and is commonly regarded as a micronutrient in food, beverages, and pharmaceutical formulations. However, abnormal concentrations of iodine lead to several diseases and disorders. While, its deficiency causes cretinism, stunted growth and hypothyroidism (Das et al., 2004). At the same time, an excess intake of iodine may lead to thyrotoxicosis (Fujiwara et al., 2000). Therefore, determination of the most suitable amount of iodine is very important for successful iodine supplementation. In the past, a variety of methods, such as spectrophotometry, chromatography coupled spectrophotometry, mass spectrometry, chemiluminescence and electrochemical methods have been employed for the detection

* Corresponding author. Tel.: +886 2270 17147; fax: +886 2270 25238.
** Corresponding author. Tel.: +886 3 2118800x5018; fax: +886 2118700.
E-mail addresses: smchen78@ms15.hinet.net (S.-M. Chen), blou@mail.cgu.edu.tw (B.-S. Lou).

http://dx.doi.org/10.1016/j.bios.2014.05.023
0956-5663/

of iodine (Huang et al., 2008; Arena et al., 2002). Though these methods provide satisfactory results, they are expensive and often require time-consuming sample preparation techniques.

Catalase (CAT) is a heme protein, which is considered as one of the most efficient oxidoreductase enzymes containing Fe (III)-protoporphyrin as a prosthetic group at the redox center (Murthy et al., 1981). It acts a biocatalyst and is having the ability to catalyze the disproportionation of hydrogen peroxide into oxygen and water (Lai and Bergel, 2002). Interestingly, in the immobilized state it has enormous potential applications in the food industry for food production and pasteurization, and textile industry. In the medical field it is used as a component in biosensor systems for the analysis of hydrogen peroxide (Wang et al., 1993). Though electrochemical techniques are proven to be the most valuable tools for the study of heme proteins (Wang et al., 2005), it is difficult to achieve the direct electron transfer (DET) of CAT at the bare electrode surface. To achieve the DET for CAT, various modified electrodes, such as chitosan, polyacrylammide hydrogel, methylcellulose, agarose hydrogel, collagen, and silica sol–gel electrodes have been proposed (Ammam and Fransaer, 2011; Salimi et al., 2007a, 2007b, 2007c). The stability of these electrodes and the use of highly expensive cross-linking agents are however problematic.

The rapid development of new nanomaterials and nanotechnologies has provided many new techniques for electroanalysis (Rivas et al., 2007). In recent years, functionalized MWCNTs (*f*-MWCNTs) have attracted special interest owing to their excellent properties such as large specific surface area, high mechanical strength, excellent conductivity and low production cost. *f*-MWCNTs have been used in wide range of applications, including electrical devices such as batteries, field-effect transistors, electrochemiluminescent sensors, electro mechanic resonators and electrochemical biosensors (Wang et al., 2005; Wu et al., 2007; Gradzka et al., 2013). Several methods have been developed for the covalent functionalization of CNTs through acid treatments, oxidation, esterification, amidation, radial coupling, anionic coupling, and cycloaddition reactions. The oxidation of carbon nanotubes in acidic solution creates negatively charged carboxyl groups at its surface, enabling the chemical attachment of molecules bearing amine groups (Kumar et al., 2012; Gebhardt et al., 2011; Balasubramanian and Burghard, 2005; Wang et al., 2006).

L-lysine is an essential α-amino acid with basic properties. L-lysine modified electrodes have the advantages of stability and positive surfaces, which provide sufficient number of active centers for wide application in electrocatalytic processes (Pereira et al., 2003; Anson et al., 1983). These positively charged biomolecules are very useful for improving the microenvironment around the enzyme and providing fast electron transfer (Mizutami et al., 1995; Haladjian et al., 1996).

In this work, a simple strategy to immobilize catalase (CAT) onto PLL modified *f*-MWCNT surface for the development of an amperometric hydrogen peroxide biosensor has been demonstrated for the first time. The development of a simple electrodeposition method is attractive in electrochemistry for the preparation of PLL films on *f*-MWCNT. We have described a simple and less time consuming approach to immobilize CAT onto the PLL/*f*-MWCNT surface without using any cross-linking agents. The results revealed that CAT retained its specific enzyme activity at the PLL/*f*-MWCNT surface without any denaturation. Highly biocompatible PLL film provides favorable microenvironment for CAT, allowing it to have direct electron transfer with the electrode surface through highly conductive *f*-MWCNT networks. Under optimum conditions, CAT/PLL/*f*-MWCNT/GCE provided high catalytic activity towards H_2O_2 and IO_3^-. The linear range for H_2O_2 and IO_3^- were 1×10^{-6}–3.6×10^{-3} and 0.1×10^{-6}–4.48×10^{-3}, respectively. The limit of detection (LOD) for H_2O_2 and IO_3^- limit are 8 nM and 0.02 μM, respectively. Having the advantages of excellent electrocatalytic activity, simple and less-time consuming fabrication steps, high stability and sensitivity, and biocompatibility, the as-developed biosensor holds great potential for various biosensing applications.

2. Experiments

2.1. Apparatus

Electrochemical experiments were carried out using a CHI405A electrochemical workstation (Chen Hua instruments Co., Shanghai, China). The three-electrode system consisted of a bare GCE (0.079 cm^{-2} geometrical surface area) or CAT/PLL/*f*-MWCNTs/GCE modified film as the working electrode, an Ag/AgCl as a reference electrode (saturated KCl) and a platinum wire as a counter electrode. Amperometric $i-t$ curve studies were carried out using a rotating disk electrode (RDE) with an analytical rotator AFMSRX (PINE instruments, USA). The morphology of the films was analyzed using a Hitachi S-3000 H scanning electron microscope (SEM) (Hitachi, Japan) and Being nano-instruments CSPM 4000, atomic force microscope (AFM). Elemental composition of the films was determined through Energy dispersive X-ray analysis (EDX) by using a HORIBA EMAX X-ACT (Model 51-ADD0009). UV–vis absorption spectroscopy measurements were carried out using a Hitachi U-3300 spectrophotometer. Fourier transform infrared (FTIR) spectra were obtained using a Perkin Elmer RXI spectrometer. X-ray photoelectron spectroscopy (XPS) was performed using a PHI 5000 Versa Probe equipped with an Al Kα X-ray source (1486.6 eV). Electrochemical impedance spectroscopy (EIS) analysis was performed in the frequency range of 100 mHz to 100 kHz using an electrochemical impedance analyzer (ZAHNER, Kroanch, Germany).

2.2. Materials

MWCNTs (O.D. 10–15 nm, I.D. 2–6 nm, length 0.1–10 μm) and catalase from bovine liver (4540 units mg^{-1}) were purchased from Sigma-Aldrich. L-lysine, H_2O_2 (30%), potassium iodate and 5 wt% Nafion were purchased from Shanghai Bio Life Science and Technology Co., Ltd. (Shanghai, China). The phosphate buffer solution (PBS) was prepared by mixing stock solutions of NaH_2PO_4 and Na_2HPO_4 and adjusting the pH values with either 0.1 M HCl or NaOH solutions. The stock solution for catalase was prepared in 0.05 M PBS (pH 6.5) and stored at 4 °C. All other reagents were of analytical reagent grade. Double distilled (DD) water was obtained from a Milli-Q system.

2.3. Acid treatment of MWCNTs

0.5 g of crude MWCNTs and 60 mL of 0.4 M HCl aqueous solution were mixed and sonicated in a water bath for 4 h. Then 60 mL of a 3:1 concentrated H_2SO_4/HNO_3 solution was added to the mixture and stirred for 4 h under reflux (Cao et al., 2012). After cooling to room temperature, the solution was diluted with 400 mL of DD water and vacuum-filtered through a 0.22 μm polycarbonate membrane. The obtained *f*-MWCNT solid was washed repeatedly with DD water until the pH of the filtrate became 7. The as-purified solid was dried in an oven for 12 h at 60 °C.

2.4. Fabrication of CAT/PLL/f-MWCNTs/GCE

GCE (3 mm diameter) was polished to a mirror-like surface using 0.05 μm alumina slurry followed by rinsing with water for several times. Then the GCE was cleaned in ethanol and water for 5 min using ultrasonic treatment, and dried at room temperature.

Prior to use, *f*-MWCNTs (1 mg/mL) were dispersed in DMF through ultrasonication for 20 min. Schematic representation showing the step-wise fabrication of CAT/PLL/*f*-MWCNT/GCE is provided in Scheme 1. 5 μL of the *f*-MWCNTs dispersion was dropped onto the pre-cleaned GCE and dried at room temperature. The modified GCE was then rinsed with water to remove loosely adsorbed *f*-MWCNTs. Higher amounts of *f*-MWCNTs could agglomerate on the electrode surface, affecting the catalytic activity and stability. So, we used an optimal concentration of 1 mg/mL. The *f*-MWCNT/GCE was subsequently transferred to an electrochemical cell containing 1 mM of PLL in 10 mL of PBS (pH 6). Lysine was electro-polymerized onto the *f*-MWCNT surface as reported elsewhere (Yu et al., 2012; Li et al., 2012). Ten consecutive cyclic voltammograms were obtained in the potential range −1.5 to +2.5 V (vs. Ag/AgCl reference electrode) at a scan rate of 100 mV s^{-1}. In Fig. S1, one can see an oxidation peak (+1.65 V) and a reduction peak (−0.7 V). In subsequent scans, a new oxidation peak (II_{pa}) appeared at +0.15 V, and a larger peak was observed when the scanning cycles were increased, indicating the continuous growth of the film. When scanning at high positive potential, the monomer PLL oxidized into α-amino free radicals, which initiated the polymerization. Prior to immobilization, CAT solution was prepared by dissolving 15.0 mg of CAT in 1 mL of PBS (pH 6.5). It has to be noted that CAT (pI=5.6) bears a net negative charge at this pH, which allow immobilization of CAT onto the positively charged PLL surfaces through electrostatic interactions. 10 μL of the CAT solution was dropped onto the PLL/*f*-MWCNTs/GCE and the resulting modified electrode was allowed to dry at an ambient temperature. The optimal CAT loading was determined to be 5 mg/mL by observing its redox peak current for various CAT loadings. Finally, 1.5 μL of the 0.5% Nafion solution was dropped onto the CAT surface and dried. The as-prepared CAT/PLL/*f*-MWCNT/GCE modified GCE was stored at 4 °C in a refrigerator under dry conditions when not in use.

3. Results and discussion

3.1. Morphology and elemental composition

Fig. 1 shows SEM and EDX images of *f*-MWCNT, PLL/*f*-MWCNT, and CAT/PLL/*f*-MWCNTs/ITO. It can be seen in Fig. 1A that the conducting surface of the ITO electrode is covered with defined nanotubular networks of *f*-MWCNTs. The nanotubes interconnect 3-dimensionally to form mat like structures. As displayed in Fig. 1B, thin flat sheet like PLL structures are deposited on the surface of *f*-MWCNTs. EDX results reveal that CAT/PLL/*f*-MWCNTs film is composed of nitrogen (20%) oxygen (50%) and carbon (30%) (Fig. S2). As can be seen in Fig. 1C, globular/bead like structures of CAT are more densely immobilized on the film surface, as a result *f*-MWCNTs and PLL structures are not identified.

XPS analysis was used to identify the elements present in PLL encapsulated *f*-MWCNTs. Fig. 1D shows the XPS spectrum of PLL/*f*-MWCNTs film. It is evident that defined signals are observed for the elements, C and O, which are assigned for *f*-MWCNTs and PLL. C 1s and O 1s peaks are found at 284.79 eV and 532.92 eV in the oxidized *f*-MWCNTs. Due to the presence of amino groups in PLL, an N 1s peak emerged at 400.83 eV (Xu et al., 2000). XPS results reveal that PLL is coated onto the surfaces of *f*-MWCNTs. The morphology and the roughness of the *f*-MWCNT electrodes surface without and with PLL films deposited during different cycles was imaged using AFM technique, with results showing that these MWCNT sheets could function as effective electrodes for the electrodeposition of PLL films (see Fig. S12 and the text for more detailed explanation).

3.2. FTIR, UV–vis spectra and EIS analysis

FTIR spectra results were used to access the nature of the interactions between the CAT and PLL/*f*-MWCNTs. As can be seen in Fig. 2A(c), characteristic peaks of amide I (1620–1680 cm^{-1}), amide II (1480–1580 cm^{-1}) and amide III (1225–1300 cm^{-1}) for CAT are found in the FTIR spectra of PLL/*f*-MWCNTs and native CAT. This indicates that CAT retains its native structure even after immobilized on the PLL/*f*-MWCNT film. The good biocompatibility of the CAT entrapped in the PLL/*f*-MWCNT film can be attributed to its high surface area, and highly active sites, which are useful for binding the CAT (Eberhardt et al., 2004; Song et al., 2011; Periasamy et al., 2011). FTIR spectra of *f*-MWCNTs and PLL/*f*-MWCNTs further confirm that *f*-MWCNTs were successfully functionalized with carboxyl groups and further it was combined with PLL via strong imide bond linkage (Fig. S3).

UV–vis spectroscopy is another effective technique used to study the positions and shapes of the Soret absorption bands, which provide information regarding possible denaturation of the heme proteins. Fig. 2B shows the UV–vis spectra of (a) CAT, (b) CAT/PLL, (c) CAT/*f*-MWCNT and (d) CAT/PLL/*f*-MWCNT. The Soret absorption band of CAT is observed at 395 nm for CAT/PLL/*f*-MWCNT (Salimi et al., 2007a, 2007b, 2007c; Lu et al., 2003) and native CAT, showing that CAT entrapped in the PLL/*f*-MWCNTs film retained its bioactivity. CAT immobilized at PLL and *f*-MWCNT films exhibit similar Soret band, without any shifts, revealing that CAT retains its bioactivity at these films.

Electrochemical impedance spectroscopy (EIS) is an important technique used to monitor the changes in the electrical properties

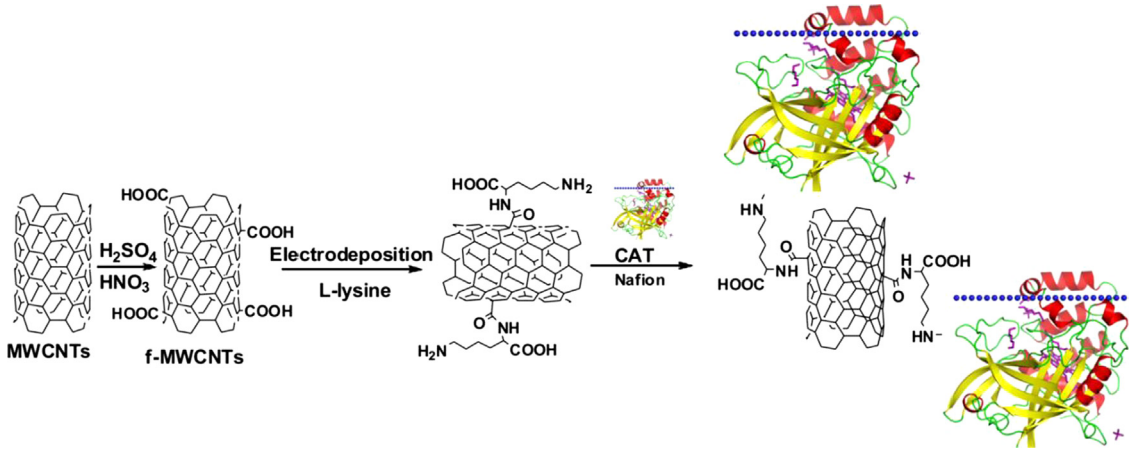

Scheme 1. Schematic illustration of the preparation of CAT/PLL/*f*-MWCNT film modified glassy carbon electrode.

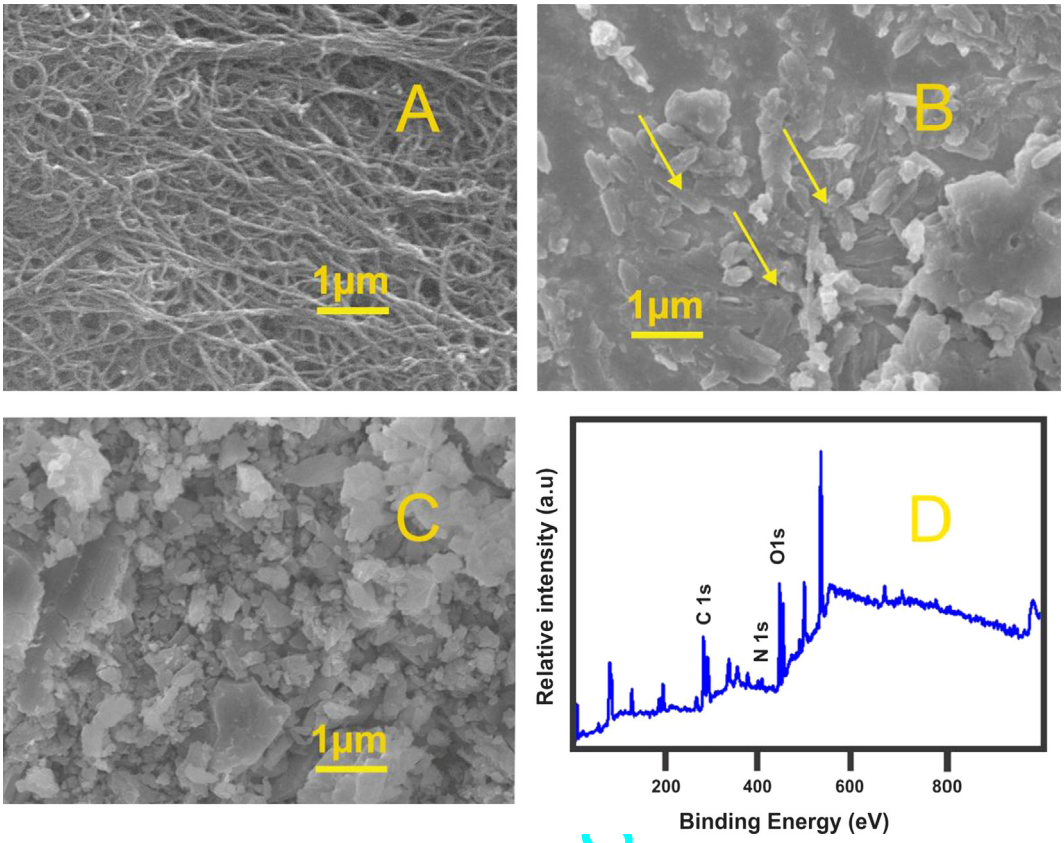

Fig. 1. SEM images of (A) *f*-MWCNT, (B) PLL/*f*-MWCNT, (C) CAT/PLL/*f*-MWCNT, and (D) XPS spectra of PLL-*f*-MWCNT films.

of the modified electrodes. The Nyquist plot displays two kinds of regions, a semicircular region at higher frequencies corresponding to the electron-transfer resistance (R_{et}) and a linear region at lower frequencies corresponding to the diffusion process. Fig. S4 illustrates the real and imaginary parts of the EIS for bare GCE, *f*-MWCNT/GCE, and PLL/GCE in pH 6.5 PBS solution containing 5 mM $Fe(CN)_6^{3-/4-}$. The inset to Fig. S4 represents the Randles circuit. The resistance to charge transfer (R_{et}) is found to be parallel to the interfacial capacity (C_{dl}). This parallel structure of R_{et} and C_{dl} gives rise to the semicircle in the complex plane plot of Z_{im} against Z_{re}. Curves (a) and (b) in Fig. S4 show the EIS spectra of bare GCE and MWCNT/GCE. The plot for the bare GCE has a semicircular domain with an electron transfer resistance (R_{et}) of 380 Ω. After modification, the R_{et} value decreases to 190 Ω, indicating that the MWCNT promotes electron transfer. Moreover, the change in R_{et} also confirms the successful immobilization of MWCNT on the surface of the GCE (Fig. S4c). shows that the PLL electrode exhibits an almost straight line, which is characteristic of the diffusion limited electrochemical process. Fig. S5 shows the typical EIS results for PLL/*f*-MWCNT/GCE, CAT/PLL/*f*-MWCNT/GCE, and CAT/GCE. Obviously, the whole EIS profile of CAT/GCE exhibits a largest semicircle, indicating a sluggish electron transfer process (curve (c)). The diameter of the semicircle for CAT/PLL/*f*-MWCNT/GCE was higher than that of PLL/*f*-MWCNTs/GCE, confirming that CAT was successfully immobilized onto the PLL/*f*-MWCNT film (curves (b) and (a)). Furthermore, increase in the R_{et} value is attributed to the electrostatic repulsion between negatively charged $Fe(CN)_6^{3-/4-}$ probe and negatively charged CAT and Nafion films. Thus, EIS results confirmed that the conductivity of the GCE has been increased by the modification with the PLL/*f*-MWCNTs/GCE and further proved that the CAT was immobilized on the modified film.

3.3. Direct electrochemistry of CAT

Fig. 3A shows the cyclic voltammograms for (a) bare (b) PLL/GCE, (c) CAT/PLL/GCE, (d) PLL/*f*-MWCNT/GCE, and (f) CAT-PLL/*f*-MWCNT film modified GCE electrodes in a 0.05 M deoxygenated phosphate buffer solution (pH 6.5) at a scan rate of 50 mV s^{-1}. A pair of well-defined and reversible redox peaks for the direct electron transfer of CAT could be observed for the PLL/*f*-MWCNT/GCE electrode, as shown in Fig. 3A(d). No redox peaks were observed for the bare glassy carbon electrode. It only displayed a small background current. Similarly, no redox peaks were observed for the CAT modified GCE. It can be seen that the background current of the PLL/*f*-MWCNT/GCE electrode is higher than that of the PLL/GCE or bare GCE (see Fig. 3A(d)), which are due to the participation of the loaded *f*-MWCNT. The results suggested that the presence of *f*-MWCNT on PLL and GCE surface had great improvement on the electrochemical response, which was partly due to excellent properties of MWCNTs such as good electrical conductivity, high chemical stability and high surface area. The higher currents in the cyclic voltammogram of the PLL/*f*-MWCNT/GCE electrode show the high conducting nature and increased active surface area at PLL/f-MWCNT/GCE. Fig. 3A(c) shows slight and poorly defined redox peaks for the CAT/PLL/GCE modified electrode, mainly because the prosthetic group of CAT is deeply seated and is not easily accessible. In contrast, the CAT/PLL/*f*-MWCNTs/GCE modified electrode exhibited stable, well-defined and reversible redox peaks, which are in accordance with the $Fe^{(III/II)}$ redox process (Saadati et al., 2012; Periasamy et al., 2011).This result indicates that *f*-MWCNT facilitates the electron transfer between the electroactive center of the CAT and the electrode. The anodic peak potential (E_{pa}) and cathodic peak potential (E_{pc}) of the redox peaks of CAT are located at −0.458 and −0.484 V, respectively. Fig. 3A The peak potential separation (ΔE_p) was found to be 26 mV. The CAT/PLL/*f*-MWCNT/GCE electrode underwent a faster electron transfer process than that of CAT/PLL/GCE, as evidenced with its much higher ΔE_p

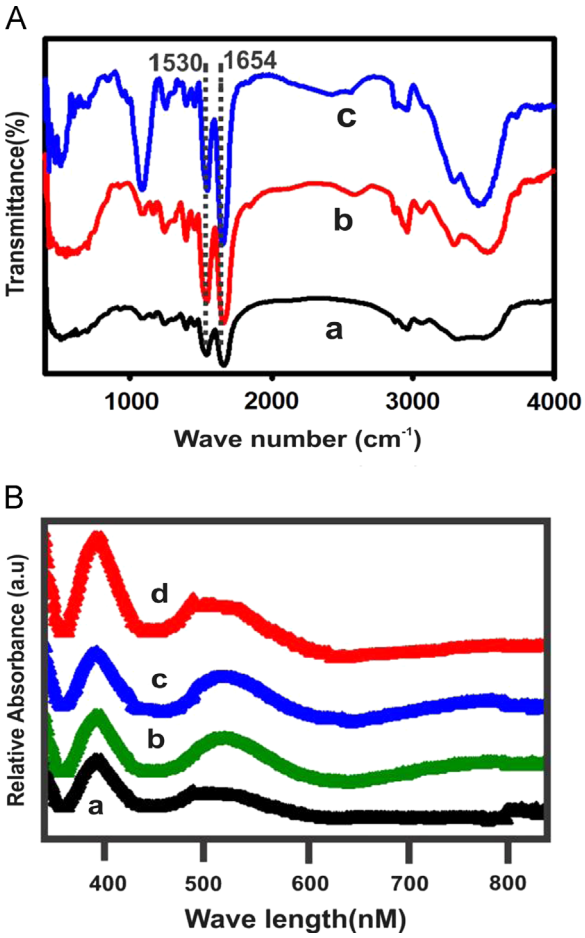

Fig. 2. (A) FTIR spectra of dry (a) CAT, (b) CAT/PLL, (c) CAT/PLL/*f*-MWCNT films. (B) UV–vis spectra of (a) CAT, (b) CAT/PLL, (c) CAT/*f*-MWCNT and (d) CAT/PLL/*f*-MWCNT.

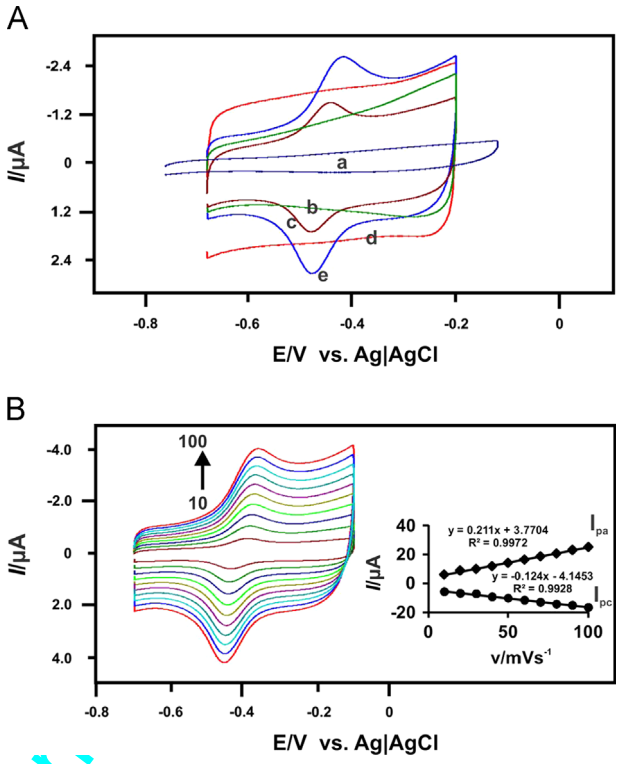

Fig. 3. (A) CVs of (a) bare (b) PLL/GCE, (c) CAT/PLL/GCE, (d) PLL/*f*-MWCNT/GCE, (f) CAT-PLL/*f*-MWCNT in 0.05 M deoxygenated PBS at a scan rate of 50 mV s^{-1}. (B) CVs of CAT/PLL/*f*-MWCNT/GCE in 0.05 M deoxygenated PBS (pH 6.5) at different scan rates (from inner to outer: 10–100 mV s^{-1}). Inset: (*I*) linear dependence of I_{pa} and I_{pc} on scan rates.

value of 40 mV. The formal potential (E'), calculated from the average value of the anodic and cathodic peak potentials is found to be −0.471 V. The positively charged PLL film provides suitable microenvironment for the negatively charged CAT, which allows it to retain its activity. The positively charged PLL film interconnects the negatively charged CAT and *f*-MWCNT films to form a sandwich like architecture, enabling the direct electron transfer between the electroactive centers of CAT and the modified electrode. The efficient immobilization of CAT at the PLL/*f*-MWCNT/GCE surface greatly increased the electroactive sites and adsorption areas, promoting electron transfer for the reduction of IO_3^- and H_2O_2.

3.4. Effects of scan rate

The electrochemical behavior of the CAT/PLL/*f*-MWCNT/GCE was studied using different scan rates in PBS pH 6.5 solution. From Fig. 3B, it can be seen that the anodic and cathodic peak currents increased with the scan rates, exhibiting a linear relationship over 10–100 mV s^{-1} (linear regression equation: anodic peak, $y=0.211x+3.7704$, $r=0.9972$; cathodic peak, $y=-0.124x-4.1453$, $r=0.9928$). Both I_{pa} and I_{pc} increased linearly with the increase of the scan rates showing that the redox process of CAT at the modified electrode is a surface-controlled process. The surface coverage of the enzyme (Γ) at the modified electrode was calculated using equation (Salimi et al., 2007a, 2007b, 2007c)

$$I_p = n^2F^2vA\Gamma/4RT \quad (1)$$

where n is the number of electrons involved, A (cm^2) is the surface area of the electrode and ν (V s^{-1}) is the scan rate. The constants R, T and F represent their usual meanings, $R=8.314$ J K^{-1} mol^{-1}, $T=298$ K, and $F=96{,}485$ C mol^{-1}. Using the slope of the plot between the scan rate and peak currents from the above equation, the surface coverage of the enzyme CAT was calculated to be 4.072×10^{-10} mol cm^{-2}. The high Γ value reveals high enzyme loading at the modified electrode. The modification of PLL onto *f*-MWCNTs increased the surface area, increasing the amounts of enzyme to be immobilized on the modified electrode. The amount of electro active CAT on the electrode surface (Γ) was calculated to be 4.072×10^{-10} mol cm^{-2}, which is higher than that of CAT PAM (2.36×10^{-11} mol cm^{-2}) (Lu et al., 2003), CAT-MC (2.36×10^{-11} mol cm^{-2}) (Li et al., 2004), CAT-silk fibroin films (6.27×10^{-11} mol cm^{-2}) (Wu et al., 2006), CAT-PNM (1.43×10^{-11} mol cm^{-2}) (Wang et al., 2007), GCE/graphene–NH_2/AuNP/CAT (0.333×10^{-11} mol cm^{-2}) (Huang et al., 2011), and GC/MWCNTs/NiO/CAT (0.153×10^{-11} mol cm^{-2}), respectively (Shamsipur et al., 2012). The high amount of CAT loaded onto the PLL/*f*-MWCNT/GCE modified film revealed the good affinity of the composite film towards CAT. The electron transfer rate constant (k_s) was calculated from the peak potential separation value using the model of Laviron (1979) (where $n\Delta E_p > 0.200$ V):

$$\log K_s = \alpha\log(1-\alpha)+(1-\alpha)\log\alpha-\log(RT/nF\nu)-\alpha(1-\alpha)nF\Delta E_p/2.3RT \quad (2)$$

here α is the charge transfer coefficient (~0.5) and the other parameters have their usual meanings. The k_s value for the PLL/*f*-MWCNT/GCE modified GCE was calculated to be 5.48 s^{-1}, which was higher than that for the CAT-MC (2.9 s^{-1}) (Li et al., 2004), CAT-silk fibroin films (0.337 s^{-1}) (Wu et al., 2006), GCE/graphene–NH_2/AuNPs/CAT (2.34 s^{-1}) (Huang et al., 2011), GC/MWCNTs/NiO/CAT (1.6 s^{-1})

(Shamsipur et al., 2012). The high k_s value indicates faster electron transfer between the active sites of CAT and the PLL/*f*-MWCNT/GCE modified electrode.

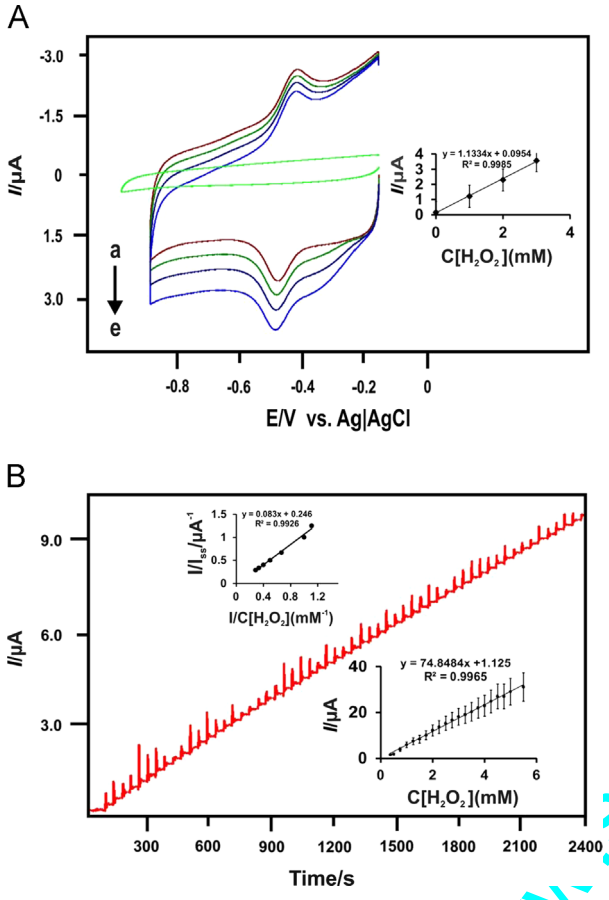

Fig. 4. Bioelectrocatalysis of the CAT/PLL/*f*-MWCNT/GCE towards H_2O_2 in PBS at a scan rate of 0.5 mV s^{-1}. H_2O_2 concentrations: (b) 0; (c) 1; (d) 2, and (e) 3 mM. (a) Bare GCE in the presence of 3 mM H_2O_2. Inset: calibration curve of the biosensor. (B) Typical current–time response curves of the CAT/PLL/*f*-MWCNT/GCE upon successive additions of H_2O_2 into pH 6.5 PBS. Applied potential: −0.45 V (vs. Ag/AgCl). Inset: calibration curve of the biosensor for H_2O_2 determination.

3.5. Electrocatalysis of H_2O_2

Apparently, the good biocompatibility and abundant edge sites of the CAT/PLL/*f*-MWCNTs/GCE composite film offer great advantages for the fabrication of a mediator-free biosensor. Fig. 4A shows the electrocatalytic activity of the CAT/PLL/*f*-MWCNT/GCE towards H_2O_2 in pH 6.5 PBS. Upon adding H_2O_2 into PBS, the reduction peak current increased linearly with increase in H_2O_2 concentrations (0–3 mM), which confirmed the excellent catalytic activity of the CAT/PLL/*f*-MWCNT/GCE modified electrode for H_2O_2 reduction. This suggests the obvious electrocatalytic behaviors of CAT entrapped in PLL/*f*-MWCNT/GCE films for the reduction of H_2O_2. The catalytic responses of (a) CAT/GCE, (b) CAT/PLL/GCE, (c) CAT/*f*-MWCNT/GCE, and (d) CAT-PLL/*f*-MWCNT/GCE for 3 mM H_2O_2 in N_2-saturated 0.05 M PBS (pH 6.5) at the scan rate of 100 mV s^{-1} are shown in Fig. S6. As we know, the reduction of H_2O_2 requires very high negative over potentials at CAT/GCE and thus no obvious redox peaks were observed in this electrochemical window (curve (a)). When the surface of the electrode was modified with the CAT/PLL/GCE electrode, an electrocatalytic reduction peak for H_2O_2 was found at 0.42 V (curve (b)). The peak was rather broad due to the slow electron transfer kinetics of H_2O_2 reduction process. In comparison with those on the CAT/GCE and CAT/PLL/GCE, a remarkable increase in reduction current and positive shift of the peak potential can be observed at the CAT/*f*-MWCNT/GCE (curve (c)), however it have less electrocatalytic activity than that of CAT/PLL/*f*-MWCNT modified GCE. All these observations indicate the excellent electrocatalytic capability of the CAT/PLL/*f*-MWCNT modified GCE toward the reduction of H_2O_2 (Fig. S6, curve (d)). The reduction peak current of the CAT/PLL/*f*-MWCNT modified GCE was 2-fold higher than that of the CAT/*f*-MWCNT/GCE. We speculate that the high surface area of PLL/*f*-MWCNT films increased the CAT immobilization, facilitating faster electron-transfer kinetics of the H_2O_2 reduction reaction and the electrocatalytic activity. Furthermore, Fig. S7 shows the stability results for CAT/PLL/*f*-MWCNT/GCE. The reduction peak current at the CAT/PLL/*f*-MWCNT/GCE was measured after recording 100 cycles in 10 μM H_2O_2. There is only a 3% decrease in the current density even after 100 cycles, indicating the good stability of CAT/PLL/*f*-MWCNT/GCE.

The amperometric detection of H_2O_2 at the CAT/PLL/*f*-MWCNT/GCE was carried out under optimal conditions. Fig. 4B shows the amperometric detection of H_2O_2 at the CAT/PLL/*f*-MWCNT modified rotating disc electrode at a rotation speed of 1200 rpm. An applied

Table 1
Comparison of electroanalytical values for various CAT modified electrodes for H_2O_2 reduction using different techniques.

Modified electrodes	Linear range (mM)	Sensitivity (μA/mM)	LOD (nM)	References
CAT[a]/AuNP[b]/graphene–NH_2/GCE	0.3–0.6	13.4	50	Huang et al. (2011)
CAT/NiO[c]/GCE	0.001–1.0	15.9	600	Salimi et al. (2007a, 2007b, 2007c)
MWCNT[d]/GCE	0.01–0.1	3.3	4000	Salimi et al. (2005)
GCE/TiNnp[e]/(CAT-IL)$_7$[f]	0.001–2.1	380	100	Saadati et al. (2012)
GCE/NF[g]/CAT/ERGO[h]	0.05–1.91	7.76	–	Ting et al. (2011)
CAT/SWNT[i]-CHI[j]/GCE	0.005–0.05	6.32	2000.5	Jiang et al. (2008)
MWCNT-NF-(DDAB[k]/CAT)	0.7–4.633	101.74	600	Prakash et al. (2009a, 2009b)
CAT/PLL/*f*-MWCNT/*GCE*	1×10^{-6}–3.6×10^{-3}	392	8	This work

[a] Catalase.
[b] Gold nanoparticles.
[c] Nickel oxide.
[d] Multi-wall carbon nanotubes.
[e] Titanium nitride nanoparticles.
[f] Ionic liquid.
[g] Nafion.
[h] Electrochemically reduced graphene oxide.
[i] Single-walled carbon nanotubes.
[j] Chitosan.
[k] Didodecyl dimethyl ammonium bromide.

potential of −0.45 V was used. H_2O_2 was sequentially injected into 0.05 M deoxygenated PBS (pH 6.5) solution (Fig. 4B). The CAT/PLL/*f*-MWCNTs/GCE modified electrode showed a good linear response towards H_2O_2. The steady-state current was reached in 5 s, indicating the fast amperometric response of the modified electrode. The calibration curve for the H_2O_2 sensor is presented in the inset to Fig. 4B. The linear range was found to be 1×10^{-6}–3.6×10^{-3}. The sensitivity and the LOD are 392 μA cm^{-2} mM^{-1}, and 8 nM ($S/N=3$), respectively. The response gradually becomes saturated at a higher H_2O_2 concentration. The detection limit, and sensitivity, obtained in this work are comparable with that of previously reported results (see Table 1). There is a linear relationship between the reciprocal of the current response ($1/I$) and the reciprocal of the H_2O_2 concentration ($1/C$) (Fig. 4B). The apparent Michaelis–Menten constant (K_M) was calculated from the Lineweaver–Burk equation (Salimi et al., 2007a, 2007b, 2007c; Periasamy et al., 2011) as follows:

$$\frac{1}{I_{ss}}=\frac{1}{I_{max}}+\frac{K_M}{I_{max}}\frac{1}{C} \quad (3)$$

where I_{ss} is the steady state current, C is the bulk concentration of the substrate and I_{max} is the maximum current under saturated substrate conditions. With the Lineweaver–Burk equation, the slope of the linear fit is used to evaluate K_M. The K_M value was calculated to be 0.224 mM, which is much smaller than that of CAT immobilized in CAT-agarose (31.7 mM) (Okuma and Watanabe, 2002), CAT-MWCNTs (1.7 mM) (Salimi et al., 2005), GCE/graphene–NH_2/AuNPs/CAT (2.81 mM) (Huang et al., 2011), and GC/TiNnp/$(CAT\text{-}IL)_7$ electrodes (1.1 mM) (Saadati et al., 2012). This result clearly suggests that CAT displays a higher affinity for H_2O_2 in the developed system.

3.6. Electrocatalytic activity of IO_3^- in PLL/f-MWCNTs

The electrocatalytic response of the PLL/*f*-MWCNT film modified GCE in pH 6.5 PBS towards IO_3^- was investigated. As shown in Fig. S8, with the addition of IO_3^-, there is a dramatic change in the electrochemical behavior of the PLL/*f*-MWCNT film modified GCE. There is an obvious increase in the reduction peak current (I_{pc}). It increased with increasing concentrations of IO_3^- (Fig. S8), showing a typical electrocatalytic reduction process of IO_3^-. However, no similar peak corresponding to the reduction of IO_3^- was observed at the bare GCE. Fig. 5A shows the amperometric response of the PLL/*f*-MWCNT film modified rotating disc GCE recorded at the rotation speed of 1000 rpm towards each addition of IO_3^- in pH 6.5 PBS. The electrode potential was kept constant at −0.72 V. It can be seen that the catalytic current increases linearly with IO_3^- concentrations over the linear range 0.1×10^{-6}–4.48×10^{-3}. From the slope of the calibration plot, sensitivity value was determined to be 2.73 mA mM^{-1} cm^{-2}. The LOD was calculated to be 0.02 μM ($S/N=3$). The electrocatalytic performance of the proposed PLL/*f*-MWCNT/GCE electrode for IO_3^- determination was compared with other modified electrodes as shown in Table S1.

3.7. Different pH studies

The effects of pH on the electrochemical behavior of the CAT/PLL/*f*-MWCNT/GCE modified electrode were investigated. A pair of well-defined and stable redox peaks was obtained for CAT in deoxygenated different pH solutions (4.5–8.5). Both the anodic and cathodic peak potentials shift towards the negative direction when increasing the pH (Ting et al., 2011). E^0 is calculated from the midpoint potential between the anodic and cathodic peaks, $E^0=(E_{pa}+E_{pc})/2$. A good linear relationship was obtained between the peak potential (E^0) and pH (Fig. 5B). The linear regression

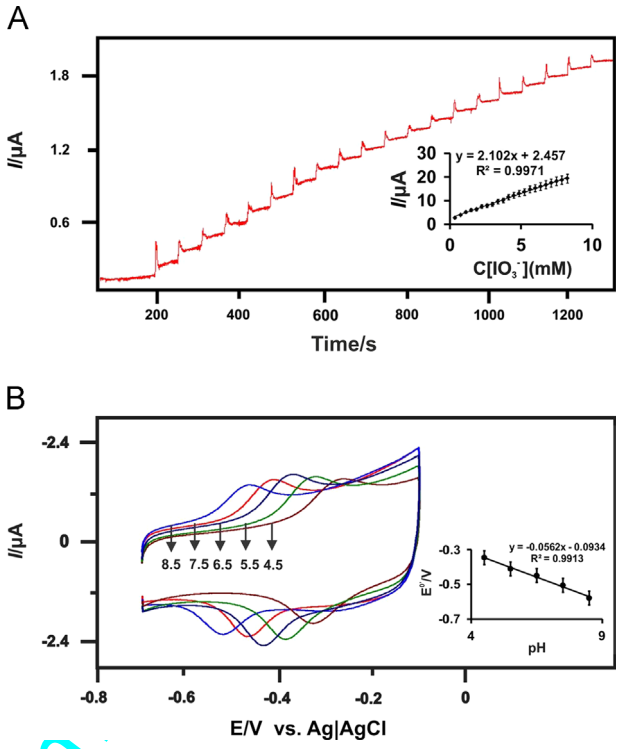

Fig. 5. (A) Amperometric response of the fabricated sensor to successive addition of IO_3^- into a stirred PBS solution (0.05 M, pH 6.5); applied potential: −0.72 V. Inset: calibration curve and linear fitting curve between the current and the IO_3^- concentration. (B) Cyclic voltammograms of the CAT/PLL/*f*-MWCNT/GCE electrode recorded in pH 4.5, 5.5, 6.5, 7.5, and 8.5. Inset: Plot of the apparent formal potentials vs. pH values. Scan rate: 0.5 mV s^{-1}.

Table 2
Electroanalytical values obtained for H_2O_2 determination in real sample using CAT/PLL/*f*-MWCNT composite film modified GCE.

Sample no.	Spiked (μM)	Found (μM)	Recovery (%)
Disinfectant cream	0.00	6.3	–
	10	14.96	101.16
Milk	0.00	59.81	–
	10	64.92	99.02

equation is expressed as follows: $E^0=-0.0562$ pH − 0.0934 ($R=0.9913$). The slope value of 56 mV/pH is close to the theoretical value of 59 mV/pH at 25 °C. This result indicates that the amount of electrons and protons transferred in the electrochemical reaction are equal. This CAT/PLL/*f*-MWCNT/GCE modified electrode can be used for electro analytical or other applications at a wide range of different pH values.

3.8. Determination of H_2O_2 in real samples

To illustrate the capability of the biosensor for practical analysis it was used to detect H_2O_2 in real samples (disinfectant cream and milk obtained from a local market). 1 mL of the real samples was diluted with PBS (pH 6.5) solution prior to use. It can be seen in Table 2 that the recovery results for the detection of H_2O_2 in disinfectant cream and milk samples are 101.16% and 99.02%, respectively. These results indicate that the CAT/PLL/*f*-MWCNT/GCE has great potential in determining H_2O_2 in real samples. Commercially available IO_3^- salt was dissolved in PBS (pH 6.5) and it was filtered prior to use. The standard addition method was adopted to demonstrate the detection of IO_3^- in real samples. The

obtained results are shown in Table S2. The good recovery results (100% and 99.96%) clearly reveal the great potential of PLL/*f*-MWCNT/GCE modified electrode for the detection of IO_3^- in real samples.

3.9. Reproducibility, repeatability and stability of CAT/PLL/f-MWCNT/GCE

To investigate the reproducibility of the proposed sensor, six CAT/PLL/*f*-MWCNT modified GCE electrodes were prepared independently and their electrocatalytic responses towards 10 μM H_2O_2 solution were measured under identical experimental conditions. The relative standard deviation (RSD) was found to be 3.26%, showing its excellent reproducibility. The repeatability of the CAT/PLL/*f*-MWCNT modified GCE examined in the presence of 10 μM H_2O_2 provided an RSD value of 3.46% ($n=8$), revealing its good repeatability. We also checked the long-term stability of the CAT/PLL/*f*-MWCNT modified GCE stored at 4 °C in pH 6.5 PBS by monitoring its response every week. The sensor retained 94.4% of its original response after 10 days, and it decreased to 89.0% after 30 days, showing its good stability. All the results reveal that the CAT/PLL/*f*-MWCNT modified GCE electrode has acceptable reproducibility and long-term stability, which make it attractive for the preparation of biosensors.

4. Conclusion

In conclusion, we developed a simple and cost-effective method for the immobilization of CAT at PLL/*f*-MWCNTs, without using any cross-linkers. The proposed PLL/*f*-MWCNT composite film provided a suitable microenvironment for the direct electrochemistry of CAT and it helps to maintain its bioactivity. The PLL/*f*-MWCNTs exhibited a large surface area and good biocompatibility with improved conductivity for the redox activity of CAT. The CAT immobilized PLL/*f*-MWCNT composite film exhibited promising catalytic activity towards H_2O_2 and IO_3^-, with higher sensitivity, lower detection limit, wide linear range and high stability.

Novelty statement

A rapid and reliable amperometric sensor for H2O2 and IO_3^- assessment was constructed through the direct electron transfer between CAT onto PLL/*f*-MWCNT/GCE.

We have used CAT/PLL/*f*-MWCNT/GCE and PLL/*f*-MWCNT/GCE modified electrode for the determination of H2O2 and IO_3^- using an amperometric method.PLL was formed by simple electrochemical deposition and the thickness of the PLL film was optimized through AFM.

The fabricated biosensor shows well good electrochemical catalytic activities toward the reaction of H2O2 and IO_3^- with excellent performance.This sensor detected H2O2 and IO_3^- over the linear range 1×10^{-6} to 3.6×10^{-3} and 0.1×10^{-6} to 4.48×10^{-3}, respectively. The limit of detection for H2O2 and IO_3^- are 8 nM and 0.02 μM, respectively.

Satisfactory stability and bioactivity were obtained for the CAT immobilized on the PLL/*f*-MWCNT/GCE modified electrode.

The proposed electrochemical sensor detected the H2O2 and IO_3^- in real samples with good recoveries.

Relative to the reported strategies, including the immobilization of CAT onto amidoxime polyacrylonitrile nanofibrous membranes (Feng et al., 2013) and covalent encapsulation of CAT onto (3-aminopropyl) trimethoxysilane (APTS) and silica nanoparticles (Yang et al., 2012), our approach is simple, less time consuming and it does not require any cross-linking reagents. It also has the advantages of enhanced operational stability, thermal stability and storage stability. PLL is relatively more biocompatible than these polymers and is having high stability in neutral pH. With more positive charges on its surface, PLL makes the negatively charged CAT to get easily immobilized on its surface.

Acknowledgment

This work was supported by the Ministry of Science and Technology, Taiwan (ROC).

Appendix A. Supplementary information

Supplementary data associated with this article can be found in the online version at http://dx.doi.org/10.1016/j.bios.2014.05.023.

References

Arena, M., Porter, M.D., Fritz, J.S., 2002. J. Anal. Chem. 74, 185–190.
Ammam, M., Fransaer, J., 2011. Sens. Actuators: B 160, 1063–1069.
Anson, F., Saveant, J., Shigehara, K., 1983. J. Am. Chem. Soc. 105, 1096–1106.
Balasubramanian, K., Burghard, M., 2005. Small 1, 180–192.
Chen, W., Cai, S., Ren, Q., Zhao, W., 2012. Analyst 137, 49–58.
Chen, S., Yuan, R., Chai, Y., Hu, F., 2013. Microchim. Acta 180, 15–32.
Cao, Q., Zhao, H., Yang, Y., He, Y., He, Y., Ding, N., Wang, J., Wu, Z., Xiang, K., Wang, G., 2012. Biosens. Bioelectron. 26, 3469–3474.
Das, P., Gupta, M., Jain, A., Verma, K., 2004. J. Chromatogr. A 1023, 33–39.
Eberhardt, A., Pedroni, V., Volpe, M., Ferreira, M., 2004. Appl. Catal. B: Environ. 47, 153–163.
Fujiwara, T., Mohammadzai, I., Inoue, H., Kumamaru, T., 2000. Analyst 125, 759–763.
Feng, Q., Wang, Q., Tang, B., Wei, A., Wang, X., Wei, Q., Huang, F., Cai, Y., Hou, D., Bi, S., 2013. Polym. Int. 62, 251–256.
Gradzka, E., Winklera, K., Borowska, M., Brzezinska, M., Echegoyen, L., 2013. Electrochim. Acta 96, 274–284.
Gebhardt, B., Syrgiannis, Z., Backes, C., Graupner, R., Hauke, F., Hirsch, A., 2011. J. Am. Chem. Soc. 133, 7985–7995.
Huang, K., Niu, D., Liu, X., Wu, Z., Fan, Y., Chang, Y., Wu, Y., 2011. Electrochim. Acta 56, 2947–2953.
Huang, X., Li, Y., Chen, Y., Wang, L., 2008. Sens. Actuators: B 134, 780–786.
Haladjian, J., Chef, I., Bianco, P., 1996. Talanta 43, 1125–1130.
Jiang, H., Yang, H., Akins, D., 2008. J. Electroanal. Chem. 623, 181–186.
Kumar, S., Kaur, I., Dharamvir, K., Bharadwaj, M., 2012. J. Colloid Interface Sci. 369, 23–27.
Lai, M., Bergel, A., 2002. Bioelectrochemistry 55, 157–160.
Li, Y., Ye, Z., Zhou, J., Liu, J., Song, G., Zhang, K., Ye, B., 2012. J. Electroanal. Chem. 687, 51–57.
Lu, H., Li, Z., Hu, N., 2003. Biophys. Chem. 104, 623–632.
Li, Y., Chen, X., Li, J., Liu, H., 2004. Electrochim. Acta 49, 3195–3200.
Laviron, E., 1979. J. Electroanal. Chem. 101, 19–28.
Mistik, S., Yukseloglu, S., 2005. Ultrasonics 43, 811–814.
Murthy, M., Reid, T., Sicignano, A., Tanaka, N., Rossmann, M., 1981. J. Mol. Biol. 152, 465–499.
Mizutami, F., Yabuki, S., Hirata, Y., 1995. Anal. Chim. Acta 314, 233–239.
Okuma, H., Watanabe, E., 2002. Biosens. Bioelectron. 17, 367–372.
Prakash, P., Yogeswaran, U., Chen, S., 2009a. Sensors 91, 1821–1844.
Prakash, P., Yogeswaran, U., Chen, S., 2009b. Talanta 78, 1414–1421.
Pereira, F., Fogg, A., Zanoni, M., 2003. Talanta 60, 1023–1032.
Periasamy, A., Ho, Y., Chen, S., 2011. Biosens. Bioelectron. 29, 151–158.
Rivas, G., Rubianes, M., Rodrıguez, M., Ferreyra, N., Luque, G., Pedano, M., Miscoria, S., Parrado, C., 2007. Talanta 74, 291–307.
Salimi, A., Noorbakhsh, A., Ghadermarzi, M., 2007a. Sens. Actuators: B 123, 530–537.
Salimi, A., Sharifi, E., Noorbakhsh, A., Soltanian, S., 2007b. Biophys. Chem. 125, 540–548.
Salimi, A., Hallaj, R., Soltanian, S., 2007c. Biophys. Chem. 130, 122–131.
Song, N., Chen, S., Huang, X., Liao, X., Shia, B., 2011. Process Biochem. 46, 2187–2193.
Shamsipur, M., Asgari, M., Mousavi, M., Davarkhah, R., 2012. Electroanalysis 24, 357–367.
Salimi, A., Noorbakhsh, A., Ghadermarz, M., 2005. Anal. Biochem. 344, 16–24.
Saadati, S., Salimi, A., Hallaj, R., Rostami, A., 2012. Anal. Chim. Acta 753, 32–41.
Tsiafoulis, C., Trikalitis, P., Prodromidis, M., 2005. Electrochem. Commun. 7, 1398–1404.
Ting, S., Periasamy, A., Chen, S., Saraswathi, R., 2011. Int. J. Electrochem. Sci. 6, 4438–4453.

Wagenaar, C., Snijders, J., 2004. Int. J. Food Microbiol. 91, 205–208.
Wael, K., Belder, S., Pilehar, S., Steenberge, G., Herrebout, W., Heering, H., 2012. Biosensors 2, 101–113.
Wang, J., Lin, Y., Chen, L., 1993. Analyst 118, 277–280.
Wang, S., Chen, T., Zhang, Z., Shen, X., Lu, Z., Pang, D., Wong, K., 2005. Langmuir 21, 9260–9266.
Wu, B., Hou, S., Yin, F., Zhao, Z., Wang, Y., Wang, X., Chen, Q., 2007. Biosens. Bioelectron. 22, 2854–2860.
Wang, C., Zhou, G., Liu, H., Wu, J., Qiu, Y., Gu, B., Duan, W., 2006. J. Phys. Chem. B 110, 10266–10271.
Wu, Y., Shen, Q., Hu, S., 2006. Anal. Chim. Acta 558, 179–186.
Wang, S., Chen, T., Zhang, Z., Pang, D., Wong, K., 2007. Electrochem. Commun. 9, 1709–1714.
Xu, S., Kumar, S., Li, Y., Jiang, N., Lee, S., 2000. J. Phys.: Condens. Matter 12, L121–L126.
Yang, S., Fu, S., Wang, M., 1991. Anal. Chem. 63, 2970–2973.
Yu, S., Cao, X., Yu, M., Yu, S., Cao, X., Yu, M., 2012. Microchem. J. 103, 125–130.
Yang, X., Cai, Z., Ye, Z., Chen, S., Yang, Y., Wang, H., Liu, Y., Cao, A., 2012. Nanoscale 4, 414–416.